

Saturation of nuclear matter and radii of unstable nuclei

Kazuhiro Oyamatsu^{a,b}, Kei Iida^b

^a*Department of Media Production and Theories, Aichi Shukutoku University, Nagakute, Nagakute-cho, Aichi-gun, Aichi 480-1197, Japan*

^b*The Institute of Physical and Chemical Research (RIKEN), Hirosawa, Wako, Saitama 351-0198, Japan*

Abstract

We examine relations among the parameters characterizing the phenomenological equation of state (EOS) of nearly symmetric, uniform nuclear matter near the saturation density by comparing macroscopic calculations of radii and masses of stable nuclei with the experimental data. The EOS parameters of interest here are the symmetry energy S_0 , the symmetry energy density-derivative coefficient L and the incompressibility K_0 at the normal nuclear density. We find a constraint on the relation between K_0 and L from the empirically allowed values of the slope of the saturation line (the line joining the saturation points of nuclear matter at finite neutron excess), together with a strong correlation between S_0 and L . In the light of the uncertainties in the values of K_0 and L , we macroscopically calculate radii of unstable nuclei as expected to be produced in future facilities. We find that the matter radii depend strongly on L while being almost independent of K_0 , a feature that will help to determine the L value via systematic measurements of nuclear size.

Key words: Dense matter, Saturation, Unstable nuclei

PACS: 21.65.+f, 21.10.Gv

1 Introduction

Saturation of density and binding energy, one of the fundamental properties of atomic nuclei, underlies a liquid-drop approach described by a Weizsäcker-Bethe mass formula [1]

$$-E_B = E_{\text{vol}} + E_{\text{sym}} + E_{\text{surf}} + E_{\text{Coul}}, \quad (1)$$

where E_B is the nuclear binding energy, E_{vol} is the volume energy, E_{sym} is the symmetry energy, E_{surf} is the surface energy, and E_{Coul} is the Coulomb energy. The sum $E_{\text{vol}} + E_{\text{sym}}$ corresponds to the saturation energy of uniform nuclear matter. Since matter in nuclei is a strongly interacting system, it remains a challenging theoretical problem to understand the nuclear matter equation of state (EOS) through microscopic calculations that utilize a model of the nuclear force duly incorporating low-energy two-nucleon scattering data and properties of light nuclei [2]. Furthermore, it is not straightforward to empirically clarify the EOS, although constraints on the EOS from nuclear masses and radii (e.g., Refs. [3–5]), observables in heavy-ion collision experiments performed at intermediate and relativistic energies (e.g., Refs. [6–9]), the isoscalar giant monopole resonance in nuclei (e.g., Ref. [10]) and even X-ray observations of isolated neutron stars [11] are available. In this work we will consider such constraints from nuclear masses and radii.

The EOS of bulk nuclear matter is a function of nucleon density n and proton fraction x , which are related to the neutron and proton number densities n_n and n_p as $n_n = n(1 - x)$ and $n_p = nx$. We may generally express the energy per nucleon near the saturation point of symmetric nuclear matter as [12]

$$w = w_0 + \frac{K_0}{18n_0^2}(n - n_0)^2 + \left[S_0 + \frac{L}{3n_0}(n - n_0) \right] \alpha^2. \quad (2)$$

Here w_0 , n_0 and K_0 are the saturation energy, the saturation density and the incompressibility of symmetric nuclear matter, S_0 is the symmetry energy $S(n)$ at $n = n_0$, $L = 3n_0(dS/dn)_{n=n_0}$ is the density symmetry coefficient, and $\alpha = 1 - 2x$ is the neutron excess. As the neutron excess increases from zero, the saturation point moves in the density versus energy plane. This movement is determined mainly by the parameters L and S_0 associated with the density-dependent symmetry energy $S(n)$ [3]. Up to second order in α , the saturation energy w_s and density n_s are given by

$$w_s = w_0 + S_0\alpha^2 \quad (3)$$

and

$$n_s = n_0 - \frac{3n_0L}{K_0}\alpha^2. \quad (4)$$

The slope, y , of the saturation line near $\alpha = 0$ ($x = 1/2$) is thus expressed as

$$y = -\frac{K_0S_0}{3n_0L}. \quad (5)$$

Derivation of L and S_0 from nuclear observables is generally obscured by the interfacial and electrostatic properties. Among the observables, the masses and root-mean-square radii of nuclei, which are controlled mainly by the bulk properties, are expected to be good tracers of L and S_0 . This expectation was stressed by an earlier investigation [3] based on two macroscopic nuclear models. Such macroscopic models are reliable in a range of neutron excess, $\alpha \lesssim 0.3$, and mass number, $A \gtrsim 50$. In this range the neutron separation energy that can be evaluated from a Weizsäcker-Bethe mass formula is greater than 2 MeV, allowing us to preclude the possibility of neutron halo formation expected at large neutron excess (or small separation energy). In constraining the EOS from masses and radii of nuclei of neutron excess $\alpha \lesssim 0.3$ and mass number $A \gtrsim 50$ within the framework of the macroscopic models, systematic study allowing for uncertainties in the EOS parameters is indispensable.

In this paper we thus explore a systematic way of extracting L and S_0 from empirical masses and radii of nuclei, together with the parameters, n_0 , w_0 and K_0 , characterizing the saturation of symmetric nuclear matter. We first set an expression for the energy of uniform nuclear matter, which reduces to the phenomenological form (2) in the limits of $n \rightarrow n_0$ and $\alpha \rightarrow 0$ ($x \rightarrow 1/2$). Using this energy expression within a simplified version of the extended Thomas-Fermi approximation, which permits us to determine the macroscopic features of the nuclear ground state, we calculate charges, charge radii and masses of β -stable nuclei. Comparing these calculations with empirical values allows us to derive the optimal parameter set for various values of the slope y and the incompressibility K_0 . We thus find a strong correlation between L and S_0 . The next step is to calculate root-mean-square charge and matter radii of more neutron-rich nuclei that are expected to be produced in future radioactive ion beam facilities. The results suggest that the density symmetry coefficient L may be constrained from possible systematic data on the matter radii in a way nearly independent of the poorly known K_0 , while the slope y being deducible as a function of K_0 . We finally discuss an empirically allowed region in the space of the parameters characterizing the EOS (2).

In Section 2 we construct a macroscopic model of nuclei. Optimization associated with fitting to empirical data for nuclei on the smoothed β -stability line is illustrated in Section 3. In Section 4 we calculate matter and charge radii of unstable nuclei. Our conclusions are presented in Section 5. Numerical tables are given in the Appendix.

2 Macroscopic description of nuclei

In constructing a macroscopic nuclear model, we begin with the expression for the bulk energy per nucleon [13],

$$w = \frac{3\hbar^2(3\pi^2)^{2/3}}{10m_n n} (n_n^{5/3} + n_p^{5/3}) + (1 - \alpha^2)v_s(n)/n + \alpha^2 v_n(n)/n, \quad (6)$$

where

$$v_s = a_1 n^2 + \frac{a_2 n^3}{1 + a_3 n} \quad (7)$$

and

$$v_n = b_1 n^2 + \frac{b_2 n^3}{1 + b_3 n} \quad (8)$$

are the potential energy densities for symmetric nuclear matter and pure neutron matter, and m_n is the neutron mass. (Replacement of the proton mass m_p by m_n in the proton kinetic energy makes only a negligible difference.) For the later purpose of roughly describing the nucleon distribution in a nucleus, we incorporate into the potential energy densities (7) and (8) a low density behaviour $\propto n^2$ as expected from a contact two-nucleon interaction. Note, however, that we will focus on the EOS of nearly symmetric nuclear matter near the saturation density. We will thus determine the parameters included in Eqs. (7) and (8) in such a way that they reproduce data on radii and masses of *stable* nuclei.

In the limit of $n \rightarrow n_0$ and $\alpha \rightarrow 0$ ($x \rightarrow 1/2$), expression (6) reduces to the usual form (2) according to

$$S_0 = \frac{1}{6} \left(\frac{3\pi^2}{2} \right)^{2/3} \frac{\hbar^2}{m_n} n_0^{2/3} + (b_1 - a_1)n_0 + \left(\frac{b_2}{1 + b_3 n_0} - \frac{a_2}{1 + a_3 n_0} \right) n_0^2, \quad (9)$$

$$\begin{aligned} \frac{1}{3} n_0 L = & \frac{1}{9} \left(\frac{3\pi^2}{2} \right)^{2/3} \frac{\hbar^2}{m_n} n_0^{5/3} + (b_1 - a_1)n_0^2 + 2 \left(\frac{b_2}{1 + b_3 n_0} - \frac{a_2}{1 + a_3 n_0} \right) n_0^3 \\ & - \left[\frac{b_2 b_3}{(1 + b_3 n_0)^2} - \frac{a_2 a_3}{(1 + a_3 n_0)^2} \right] n_0^4, \end{aligned} \quad (10)$$

$$w_0 = \frac{3}{10} \left(\frac{3\pi^2}{2} \right)^{2/3} \frac{\hbar^2}{m_n} n_0^{2/3} + a_1 n_0 + \frac{a_2 n_0^2}{1 + a_3 n_0}, \quad (11)$$

$$K_0 = -\frac{3}{5} \left(\frac{3\pi^2}{2} \right)^{2/3} \frac{\hbar^2}{m_n} n_0^{2/3} + \frac{18a_2 n_0^2}{(1 + a_3 n_0)^3}, \quad (12)$$

$$0 = \frac{1}{5} \left(\frac{3\pi^2}{2} \right)^{2/3} \frac{\hbar^2}{m_n} n_0^{-1/3} + a_1 + \frac{2a_2 n_0}{1 + a_3 n_0} - \frac{a_2 a_3 n_0^2}{(1 + a_3 n_0)^2}. \quad (13)$$

Equation (13) comes from the fact that the density derivative of the energy per nucleon at $n = n_0$ and $\alpha = 0$ ($x = 1/2$) vanishes due to the saturation. Note that the five relations (9)–(13) are not sufficient to determine the six parameters a_1, \dots, b_3 , and that the parameter b_3 , which controls the EOS of matter at large neutron excess and high density, has little effect on the saturation properties of nearly symmetric nuclear matter. We will thus set b_3 as a typical value 1.58632 fm^3 , which was obtained by one of the authors [13], and determine the other parameters from the empirical radii and masses of stable nuclei.

We now proceed to describe a spherical nucleus of proton number Z and mass number A within the framework of a simplified version of the extended Thomas-Fermi theory [13]. We first write the total energy of a nucleus as a function of the density distributions $n_n(\mathbf{r})$ and $n_p(\mathbf{r})$ according to

$$E = E_b + E_g + E_C + Nm_n + Zm_p, \quad (14)$$

where

$$E_b = \int d^3r n(\mathbf{r}) w(n_n(\mathbf{r}), n_p(\mathbf{r})) \quad (15)$$

is the bulk energy,

$$E_g = F_0 \int d^3r |\nabla n(\mathbf{r})|^2 \quad (16)$$

is the gradient energy with an adjustable constant F_0 ,

$$E_C = \frac{e^2}{2} \int d^3r \int d^3r' \frac{n_p(\mathbf{r})n_p(\mathbf{r}')}{|\mathbf{r} - \mathbf{r}'|} \quad (17)$$

is the Coulomb energy, and $N = A - Z$ is the neutron number. Here we ignore shell and pairing effects. We also neglect the contribution to E_g from the gradient of the proton fraction x [see Eq. (16)]; this contribution makes only a little difference even in the description of extremely neutron-rich nuclei, as clarified in the context of neutron star matter [13].

The energy (14), once optimized, can be mapped onto a Weizsäcker-Bethe mass formula of the form (1) via

$$E_{\text{surf}} = E_g + (E_b - E_{\text{vol}}) + (E_C - E_{\text{Coul}}), \quad (18)$$

where $E_b - E_{\text{vol}}$ denotes the inhomogeneity contribution to the bulk energy E_b , and $E_C - E_{\text{Coul}}$ ($E_{\text{Coul}} = 3Z^2e^2/5R$ with the liquid-drop radius R) denotes that to the Coulomb energy E_C . These inhomogeneity contributions arise from the fact that matter in a nucleus is compressible. We remark that in equilibrium with respect to nuclear size, $E_g = E_C$ holds [13]. Combining this relation with the well-known equilibrium condition for the liquid-drop size, $E_{\text{surf}} = 2E_{\text{Coul}}$, and with $E_{\text{Coul}} \simeq E_C$, we find a simple relation, $E_g \simeq E_{\text{surf}}/2$, for an equilibrium nuclide.

For the present purpose of examining the macroscopic properties of nuclei such as masses and radii, it is sufficient to characterize the neutron and proton distributions for each nucleus by the central densities, radii and surface diffuseness different between neutrons and protons, as in Ref. [13]. We thus assume the nucleon distributions $n_i(r)$ ($i = n, p$), where r is the distance from the center of the nucleus, as

$$n_i(r) = \begin{cases} n_i^{\text{in}} \left[1 - \left(\frac{r}{R_i} \right)^{t_i} \right]^3, & r < R_i, \\ 0, & r \geq R_i. \end{cases} \quad (19)$$

Here R_i roughly represents the nucleon radius, t_i the relative surface diffuseness, and n_i^{in} the central number density. The proton distribution of the form (19) can fairly well reproduce the experimental data for stable nuclei such as ^{90}Zr and ^{208}Pb , as we shall see in the next section.

3 Optimization

For fixed mass number A , we then optimize the energy (14) with respect to the parameters R_i , t_i and n_i^{in} . (In a general Thomas-Fermi approach, such optimization is carried out without assuming a particular form of the distributions.) The resultant optimal values of charge number, nuclear mass and root-mean-square charge radius

$$R_c = \left[Z^{-1} \int d^3r r^2 \rho_c(\mathbf{r}) \right]^{1/2}, \quad (20)$$

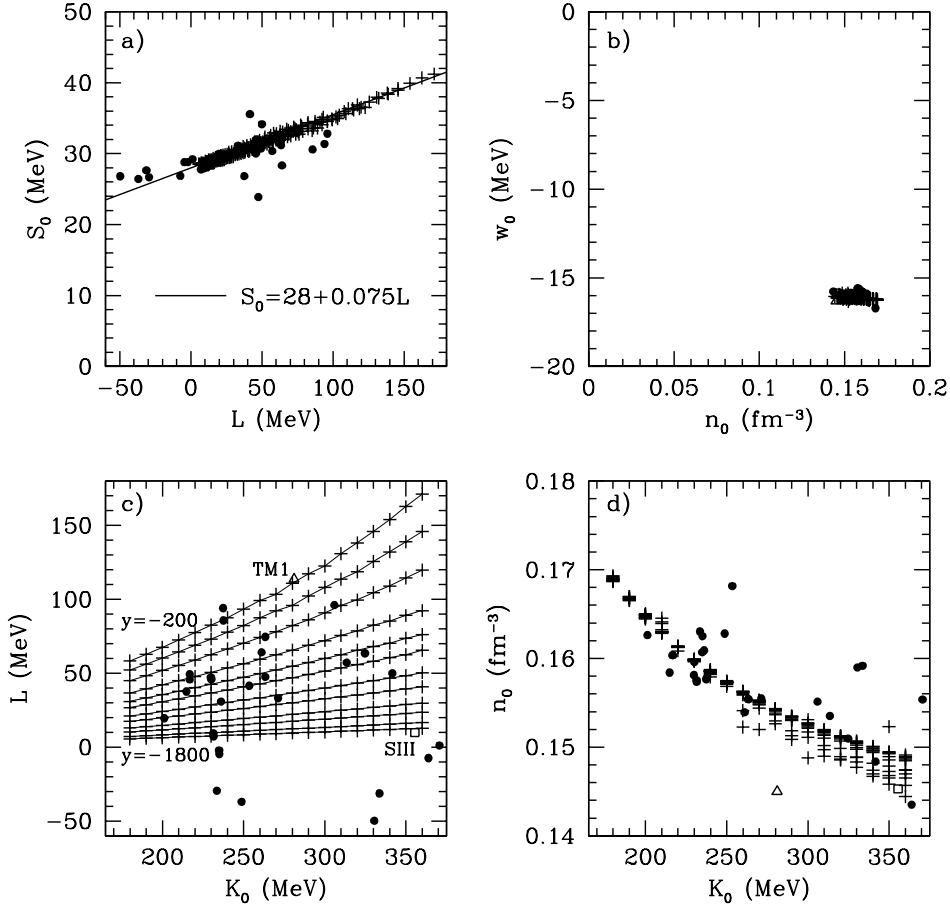


Fig. 1. Various optimal relations among the parameters S_0 , n_0 , w_0 , L and K_0 characterizing the EOS of nearly symmetric nuclear matter. In addition to the present results (crosses), the Skyrme-Hartree-Fock predictions [dots except for SIII (square)] and the TM1 prediction (triangle) are plotted. In (c), the thin lines are lines of constant y .

where

$$\rho_c(\mathbf{r}) = (\pi^{1/2}a_p)^{-3} \int d^3r' \exp(-|\mathbf{r} - \mathbf{r}'|^2/a_p^2) n_p(\mathbf{r}') \quad (21)$$

with $a_p = 0.65$ fm is the charge distribution folded with the proton form factor [14], are functions of a_1 – b_3 and F_0 . These optimal values are in turn compared with the empirical values for nuclei on the smoothed β -stability line ranging $25 \leq A \leq 245$ (see Table A.1 in Ref. [13], which is based on Refs. [15,16]). For fixed slope y and incompressibility K_0 , such a comparison can be made by a usual least squares fitting, which gives rise to an optimal set of the parameters a_1 – b_3 and F_0 . Here, we set y and K_0 as $-1800 \text{ MeV fm}^3 \leq y \leq -200 \text{ MeV fm}^3$ and $180 \text{ MeV} \leq K_0 \leq 360 \text{ MeV}$; the numerical results for n_0 , w_0 , S_0 , L and F_0 are tabulated in the Appendix. When the slope is very gentle ($0 > y \gtrsim -200$

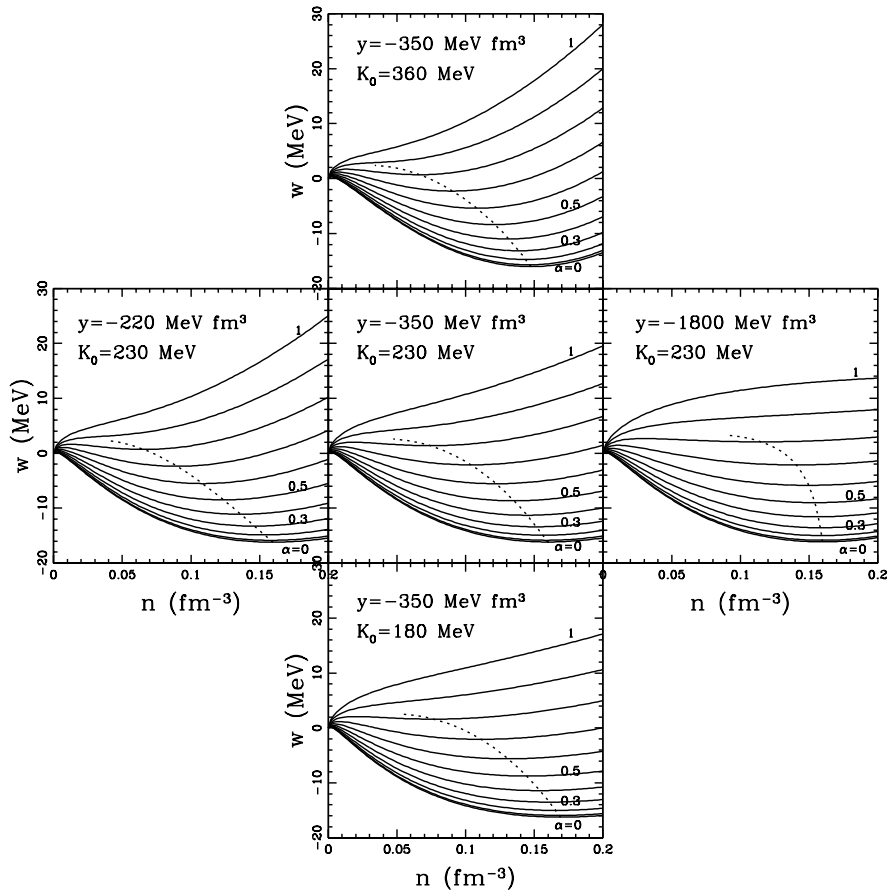


Fig. 2. The energy per nucleon as a function of nucleon density. The dotted lines denote the saturation lines.

MeV fm³), the optimal set is unavailable for large K_0 ; when the slope is very steep, the optimal parameters converge on the values close to those obtained for $y = -1800$ MeV fm³. Nuclear masses that can be calculated from the optimal parameter sets agree well with the experimental data of 1962 nuclides ($A \geq 2$) [17]; for all the combinations of y and K_0 , the root-mean-square deviations of the masses are $\sim 3\text{--}5$ MeV, which are roughly as large as those obtained from a Weizsäcker-Bethe type formula. We likewise evaluated the root-mean-square charge radii of various stable nuclei; the root-mean-square deviations from the experimental data of 92 nuclides ($A \geq 50$) [16] are about 0.06 fm.

The optimal results for S_0 , L , n_0 and w_0 are plotted in Fig. 1. From Fig. 1a, we obtain a relation nearly independent of K_0 :

$$S_0 \approx B + CL, \quad (22)$$

where $B \approx 28$ MeV and $C \approx 0.075$. We find from Figs. 1b and 1d that the saturation energy and density of symmetric nuclear matter always take on a value of -16.0 ± 0.5 MeV and 0.155 ± 0.015 fm $^{-3}$. Several data in Fig. 1d having n_0 smaller than the standard values correspond to the case of $y = -200$ MeV fm 3 , where the fitting is no longer effective. In Fig. 1c, we see a band on which the optimal values of L and K_0 are scattered; in this band L increases with increasing y for fixed K_0 . For comparison we also plot the predictions from various Skyrme-Hartree-Fock schemes (references in Ref. [4]; Refs. [18–20]) and a relativistic mean field model (TM1 in Ref. [21]); the values for n_0 , w_0 , K_0 , S_0 , L and y are tabulated in Table 1. These predictions are distributed over the band, among which only two (TM1 and SIII) were considered in the previous analysis [3]. We remark in passing that the optimal values of F_0 are confined to 66 ± 6 MeV fm 5 , consistent with the result of Ref. [13].

In Fig. 2 we display the EOS (6) for various sets of y and K_0 . Whereas y affects the slope of the saturation line, K_0 controls n_0 as well as the curvature of the line of constant α . The neutron and proton distributions in ^{208}Pb and ^{90}Zr modelled via Eq. (19) are plotted in Fig. 3. The question we consider in the next section is how such differences in the saturation properties as shown in Fig. 2 affect matter and charge radii of unstable nuclei that can be evaluated from the distributions of the form illustrated in Fig. 3.

4 Matter and charge radii

For neutron-rich nuclides we now obtain the root-mean-square charge radii R_c and matter radii R_m , defined as

$$R_m = \left[A^{-1} \int d^3r r^2 \rho_m(\mathbf{r}) \right]^{1/2}, \quad (23)$$

where

$$\rho_m(\mathbf{r}) = (\pi^{1/2} a_p)^{-3} \int d^3r' \exp\left(-|\mathbf{r} - \mathbf{r}'|^2/a_p^2\right) n(\mathbf{r}') \quad (24)$$

is the matter distribution folded with the proton charge form factor equally for neutrons and protons. We evaluated the radii R_c and R_m of Ni and Sn isotopes for combinations of $y = -220, -350, -1800$ MeV fm 3 and $K_0 = 180, 230, 360$ MeV. The results are shown at neutron excess of up to $\alpha \sim 0.4$ in Fig. 4. We find from the upper panels of Fig. 4 (see also the upper panels of Fig. 5 for further clarity) that at $\alpha \sim 0.3$ ($x \sim 0.35$) a difference of order 0.05–0.1 fm occurs in the matter radii due to variation in the slope y . This is because as the slope becomes gentler, the saturation density difference $n_0 - n_s$ becomes

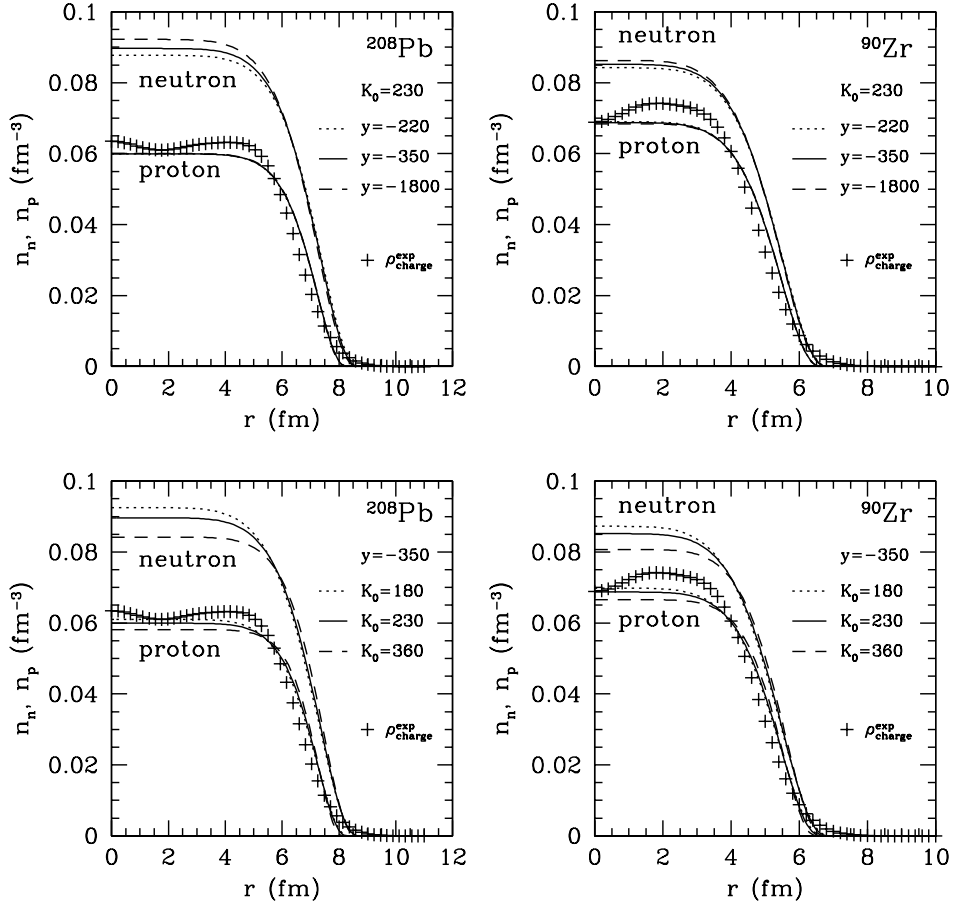


Fig. 3. The neutron and proton density distributions in ^{208}Pb and ^{90}Zr . Experimental data on the charge distributions (crosses) are taken from Ref. [16].

larger [see Eq. (4)]. We also find that the charge radii depend only weakly on y , a feature consistent with the prediction made in Ref. [3]. We can thus expect that forthcoming empirical data on matter radii of unstable neutron-rich nuclei with accuracy down to order ± 0.01 fm will at least answer the question of whether the slope y is steep or gentle.

Several remarks, however, are needed here. First, it is to be noted that the experimental matter radii that can be derived from measurements of interaction cross sections [22] and elastic scattering of protons and alpha particles [23] depend strongly on treatment of the optical potential, in contrast to the charge radii that can be determined from elastic electron scattering [16,24], muonic X-ray experiments [16,24] and isotope-shift measurements [25,24]. This dependence contributes to intrinsic uncertainties in the derived matter radii, which are typically of order or greater than ± 0.05 fm [23,26]. Second, we recall that the present calculations of the radii R_m and R_c ignore the tails of the nucleon distributions arising from quantum-mechanical effects; the absence

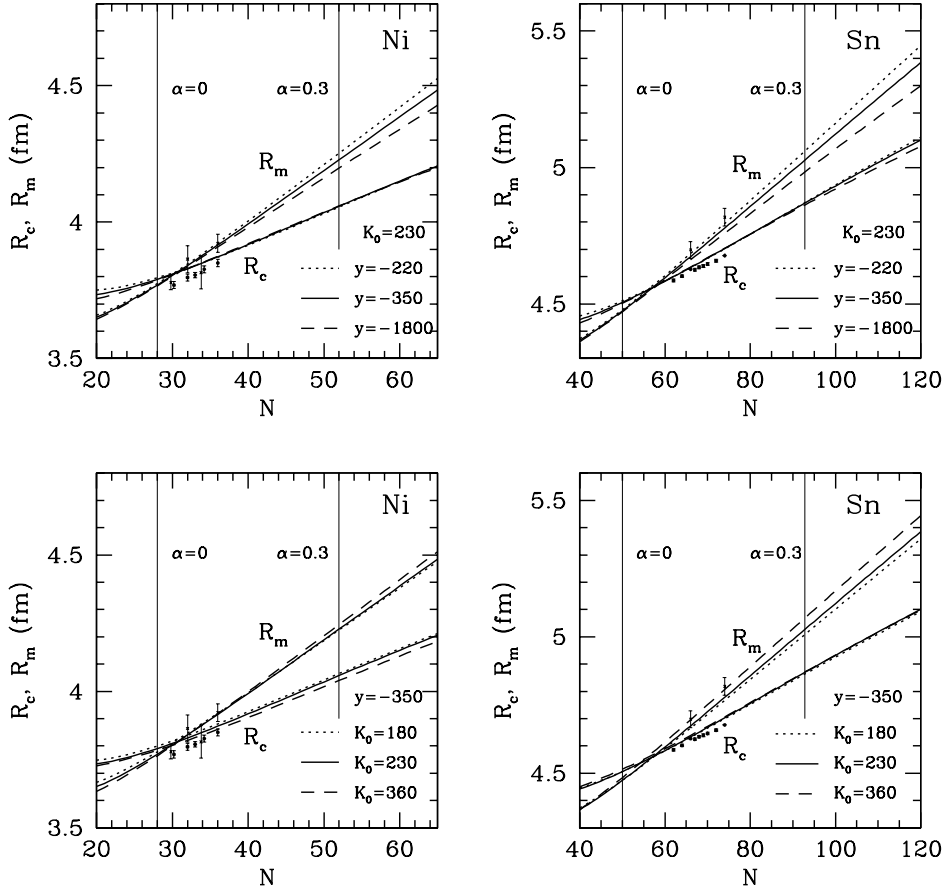


Fig. 4. The root-mean-square charge and matter radii of Ni and Sn isotopes for combinations of $y = -220, -350, -1800 \text{ MeV fm}^3$ and $K_0 = 180, 230, 360 \text{ MeV}$. Experimental data on the root-mean-square charge radii (dots) and matter radii (crosses) are taken from Refs. [16] and [23], respectively.

of such tails tends to reduce the radii. Third, there are uncertainties in the calculated radii due to the absence of shell and pairing effects in the present macroscopic models. These models, which are fitted to the charge radii of nuclei on the *smoothed* β stability line, provide the proton-closed-shell nuclei, Ni and Sn, with larger charge radii than the empirical values, as shown in Fig. 4. Fourth, we can see from the lower panels of Fig. 4 that with K_0 increased and y fixed, the matter radii R_m increase, a feature that prevents a clear derivation of y from R_m .

Such K_0 dependence of the matter radii R_m is due mainly to the K_0 dependence of the saturation density, n_s , given by Eq. (4). For fixed y , the K_0 dependence of n_s is dominated by n_0 , which increases with decreasing K_0 as in Fig. 1d. Generally, this increase in n_0 tends to increase the inner nucleon densities (see the lower panels of Fig. 3) and hence reduce the radii R_m . Note,

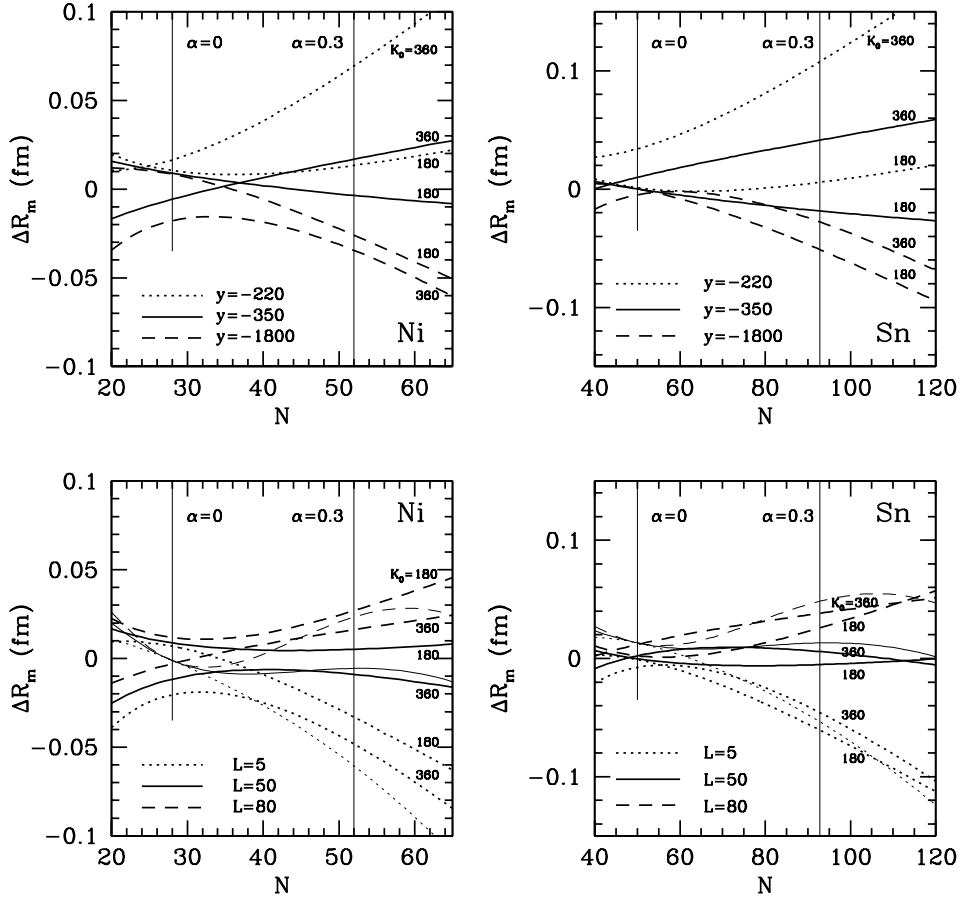


Fig. 5. Differences of the root-mean-square matter radii of Ni and Sn isotopes, ΔR_m , from those calculated for $y = -350 \text{ MeV fm}^3$ and $K_0 = 230 \text{ MeV}$ (upper panels) and for $L = 50 \text{ MeV}$ and $K_0 = 230 \text{ MeV}$ (lower panels). The thin curves in the lower panels are from formulas (26) and (27).

however, that there is an opposite effect of K_0 on R_m . This effect comes from the fact that a significant part of the nucleons are present in the deepest region of the nuclear surface where $r^2 n_n(r)$ and $r^2 n_p(r)$ are peaked. In this region, the nucleon densities begin to drop in such a way that with decreasing K_0 , the surface diffuses further away. This diffuseness, which can also be seen from the lower panels of Fig. 3, is consistent with the results from microscopic nuclear models [27].

A cancellation between those counteracting effects is favoured for the purpose of deriving information about the saturation properties in a way independent of K_0 . It turns out that better cancellation can be achieved if we calculate, as in the lower panels of Fig. 6, the matter radii of Ni and Sn isotopes for the EOS parameters optimized under fixed L rather than y . The charge radii likewise calculated are also nearly independent of K_0 . On the

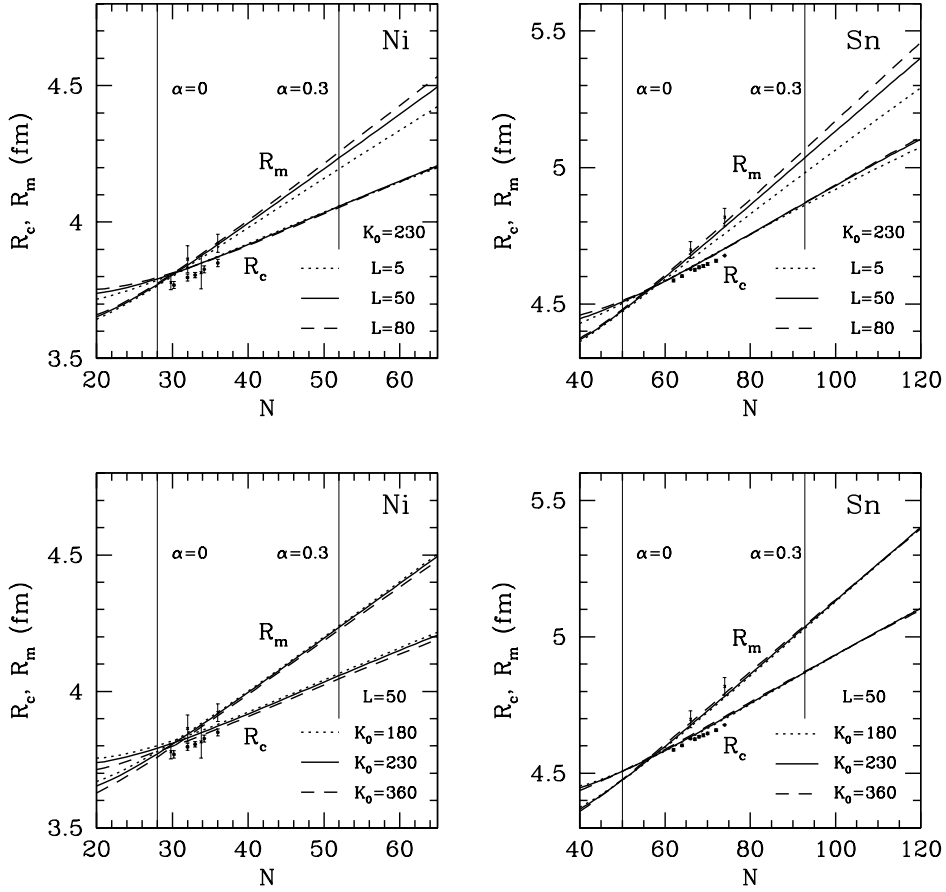


Fig. 6. Same as Fig. 4 for combinations of $L = 5, 50, 80$ MeV and $K_0 = 180, 230, 360$ MeV.

other hand, under fixed K_0 , the dependence of the matter and charge radii on L , as depicted in the upper panels of Fig. 6, is the same as that on y . These results from Fig. 6 may open an opportunity to empirically determine the density symmetry coefficient L from the isotopic dependence of matter radii.

For the purpose of parametrizing the matter and charge radii as functions of A , α and L , it is useful to first obtain fitting formulas for the root-mean-square neutron and proton radii, defined as

$$R_n = \left[N^{-1} \int d^3r r^2 n_n(r) \right]^{1/2}, \quad R_p = \left[Z^{-1} \int d^3r r^2 n_p(r) \right]^{1/2}. \quad (25)$$

To be fitted to are the radii R_n and R_p of Ni, Sn and Pb isotopes ranging $0 \leq \alpha \leq 0.3$ ($0.35 \leq x \leq 0.5$) as calculated from the present macroscopic model for the EOS parameter sets tabulated in Table A.1. In Fig. 7 the results for ^{56}Ni , ^{80}Ni , ^{116}Sn and ^{142}Ni are plotted as functions of L . We observe from

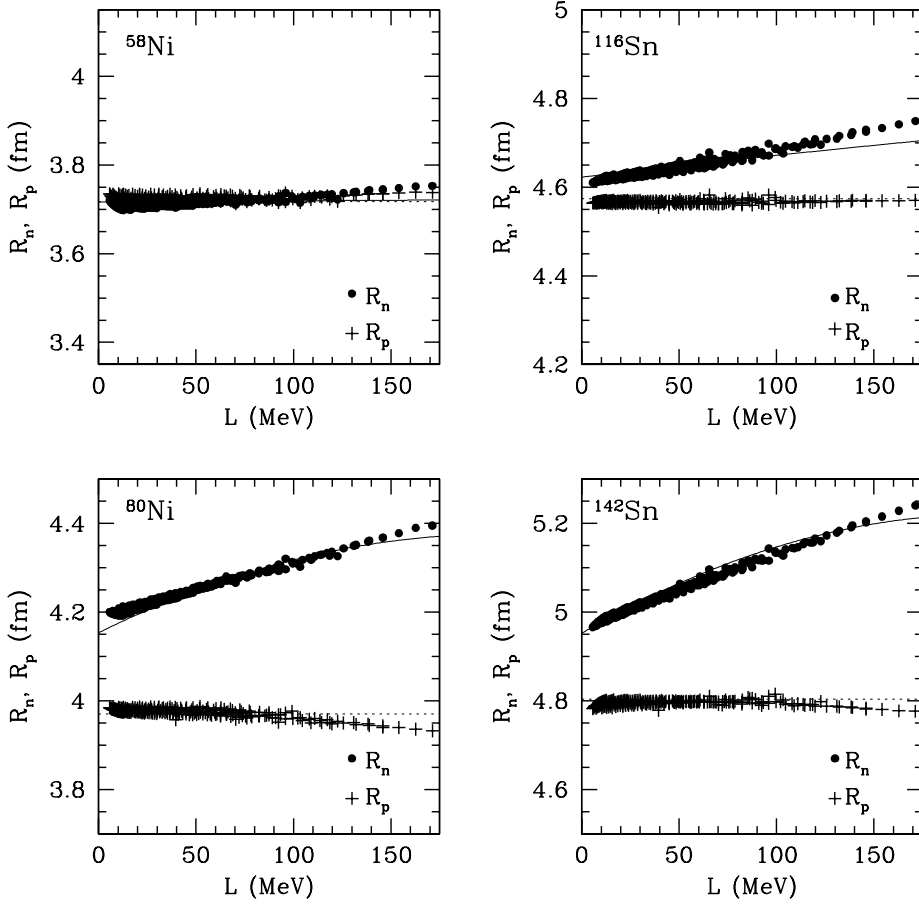


Fig. 7. The root-mean-square neutron (dots) and proton (crosses) radii of ^{58}Ni , ^{80}Ni , ^{116}Sn and ^{142}Sn for the EOS parameter sets tabulated in Table A.1. The solid and dotted lines are from formulas (27) and (26), respectively.

this figure that no uncertainties in R_p more than ± 0.03 fm arise from the various values of K_0 and L , while the K_0 dependence of R_n can be ignored as compared with the L dependence, which is stronger at larger neutron excess. These features, consistent with the dependence of R_m and R_c on L and K_0 as mentioned above, lead us to the formulas,

$$R_p = c_1 A^{1/3} + c_2 + c_3 (\alpha - \alpha_0)^2, \quad (26)$$

with $c_1 = 0.914961$ fm, $c_2 = -0.102372$ fm, $c_3 = 0.388905$ fm and $\alpha_0 = 0.879704$, and

$$R_n = c_4 A^{1/3} (1 + c_5 L \alpha^2 + c_6 L^2 \alpha^4) + c_7 + c_8 \alpha, \quad (27)$$

with $c_4 = 0.880489$ fm, $c_5 = 0.00635080$ MeV $^{-1}$, $c_6 = -0.000172275$ MeV $^{-2}$, $c_7 = 0.301616$ fm and $c_8 = 0.193326$ fm. Expressions (26) and (27) reproduce

the original values with the root-mean-square deviations of 0.010 fm and 0.013 fm, respectively, and roughly obey a usual $A^{1/3}$ law for fixed L and α . Finally, the parametrization of the matter and charge radii can be constructed from Eqs. (26) and (27) via the relations $R_m^2 = (Z/A)R_p^2 + (N/A)R_n^2 + 3a_p^2/2$ and $R_c^2 = R_p^2 + 3a_p^2/2$ that can be derived from Eqs. (20), (23) and (25).

The lower panels of Fig. 5 depict the matter radii of Ni and Sn isotopes calculated for various combinations of L and K_0 relative to those calculated for $L = 50$ MeV and $K_0 = 230$ MeV. As can be seen from these panels, K_0 -induced uncertainties in the matter radii at constant L are limited to the order of ± 0.015 fm in the neutron-rich side, small enough for the L dependence of the matter radii to be seen clearly. This may play a role in determining L from measurements of the matter radii. Note, however, that possible data on matter radii for isotopes of a specific element would be insufficient to determine the density symmetry coefficient L , as inferred from the differences between the empirical and calculated charge radii shown for Ni and Sn in Fig. 6. In view of such differences as well as intrinsic uncertainties in the matter radii that can be deduced from proton and alpha-particle elastic scattering data, systematics of the isotopic dependence of matter radii would be required.

It is interesting to note that the difference between the neutron and proton radii increases with increasing L in a way dependent on neutron excess but almost independent of K_0 (see Fig. 7). This leads us to study the isotopic dependence of neutron skin thickness in order to derive the density symmetry coefficient L . The previous investigation [3] has already suggested the possibility that the EOS of asymmetric nuclear matter will be probed by future detection of neutron skin thickness in unstable neutron-enriched nuclei. However, the neutron skin structure depends strongly on the EOS of nuclear matter at large neutron excess and low density [4], which is empirically hard to determine. Moreover, the fact [28] that the neutron skin thickness is thermodynamically relevant to the dependence of the surface tension on neutron excess complicates an extraction of the bulk properties of asymmetric nuclear matter; the connection between the surface and bulk properties remains to be clarified. We will elsewhere reinvestigate how the neutron skin thickness is phenomenologically related to the EOS of nearly symmetric nuclear matter [29].

5 Conclusion

In this paper we have derived the relations between the parameters characterizing the EOS of nearly symmetric nuclear matter from experimental data on radii and masses of stable nuclei. We have found the linear relation (22) between the parameters L and S_0 associated with the symmetry energy. It is

interesting to regard the band structure on the K_0 versus L plane (see Fig. 1c) as an empirically allowed region of K_0 and L . Future systematic measurements of the root-mean-square matter radii of unstable neutron-rich nuclei may narrow the allowed region in such a way as to fix L almost independently of K_0 . Once L is determined, the slope y would be given as a function of K_0 . It is instructive to note that the incompressibility was estimated to be $K_0 = 231 \pm 5$ MeV from the observations of the giant monopole resonances [10]. This estimate can stringently limit the allowed region, although it is model-dependent in the sense that it involves microscopic calculations of the resonance energies from a specific model of the effective nucleon-nucleon interactions [30].

Acknowledgements

We are grateful to I. Tanihata, T. Suda, A. Ozawa, A. Kohama, H. Nakada, Y. Mochizuki and H. Koura for helpful discussions. Author KO would like to thank Y. Mochizuki for hospitality during the course of this research at RIKEN. This work was supported in part by RIKEN Special Postdoctoral Researchers Grant No. 011-52040.

Appendix: Evaluation of the parameters in Eq. (2)

In this appendix we tabulate (Table A.1) the optimal values of various EOS parameters in Eq. (2).

References

- [1] J.M. Blatt and V.F. Weisskopf, *Theoretical Nuclear Physics*, Wiley, New York, 1952.
- [2] H. Heiselberg, V.R. Pandharipande, *Ann. Rev. Nucl. Part. Sci.* 50 (2000) 481.
- [3] K. Oyamatsu, I. Tanihata, Y. Sugahara, K. Sumiyoshi, H. Toki, *Nucl. Phys. A* 634 (1998) 3.
- [4] B.A. Brown, *Phys. Rev. Lett.* 85 (2000) 5296.
- [5] K.C. Chung, C.S. Wang, A.J. Santiago, *nucl-th/0102017*.
- [6] B.A. Li, *Phys. Rev. Lett.* 85 (2000) 4221.
- [7] C. Sturm et al., *Phys. Rev. Lett.* 86 (2001) 39.

- [8] C. Fuchs, A. Faessler, E. Zabrodin, Y.M. Zheng, *Phys. Rev. Lett.* 86 (2001) 1974.
- [9] P. Danielewicz, in: *Proc. Int. Symp. on Non-Equilibrium and Nonlinear Dynamics in Nuclear and Other Finite Systems*, Beijing, 2001, nucl-th/0112006.
- [10] D.H. Youngblood, H.L. Clark, Y.-W. Lui, *Phys. Rev. Lett.* 82 (1999) 691.
- [11] J.A. Pons, F.M. Walter, J.M. Lattimer, M. Prakash, R. Neuhaeuser, *P. An, Astrophys. J.* 564 (2002) 981.
- [12] J.M. Lattimer, *Ann. Rev. Nucl. Part. Sci.* 31 (1981) 337.
- [13] K. Oyamatsu, *Nucl. Phys. A* 561 (1993) 431.
- [14] L.R.B. Elton, A. Swift, *Nucl. Phys. A* 94 (1967) 52.
- [15] M. Yamada, *Prog. Theor. Phys.* 32 (1964) 512.
- [16] H. de Vries, C.W. de Jager, C. de Vries, *At. Data Nucl. Data Tables* 36 (1987) 495.
- [17] G. Audi, A.H. Wapstra, *Nucl. Phys. A* 595 (1995) 409.
- [18] S. Goriely, F. Tondeur, J.M. Pearson, *At. Data Nucl. Data Tables* 77 (2001) 311.
- [19] M. Samyn, S. Goriely, P.-H. Heenen, J.M. Pearson, F. Tondeur, *Nucl. Phys. A* 700 (2002) 142.
- [20] E. Chabanat, P. Bonche, P. Haensel, J. Meyer, R. Schaeffer, *Nucl. Phys. A* 635 (1998) 231.
- [21] Y. Sugahara, H. Toki, *Nucl. Phys. A* 579 (1994) 557.
- [22] A. Ozawa, T. Suzuki, I. Tanihata, *Nucl. Phys. A* 693 (2001) 32.
- [23] C.J. Batty, E. Friedman, H.J. Gils, H. Rebel, *Adv. Nucl. Phys.* 19 (1989) 1.
- [24] G. Fricke, C. Bernhardt, K. Heilig, L.A. Schaller, L. Schellenberg, E.B. Shera, C.W. de Jager, *At. Data Nucl. Data Tables* 60 (1995) 177.
- [25] G. Huber et al., *Phys. Rev. C* 18 (1978) 2342.
- [26] L. Ray, G.W. Hoffmann, W.R. Coker, *Phys. Rep.* 212 (1992) 223.
- [27] S. Yoshida, H. Sagawa, N. Takigawa, *Phys. Rev. C* 58 (1998) 2796.
- [28] C.J. Pethick, D.G. Ravenhall, *Nucl. Phys. A* 606 (1996) 173.
- [29] K. Iida, K. Oyamatsu, unpublished.
- [30] J.P. Blaizot, J.F. Berger, J. Dechargé, M. Girod, *Nucl. Phys. A* 591 (1995) 435.

Table 1
The saturation properties of nuclear matter obtained from various effective forces

Force	n_0	$-w_0$	K_0	S_0	L	$-y$
SI	0.155	16.0	371	29.2	1.18	19700
SII	0.148	16.0	342	34.2	50.0	524
SIII	0.145	15.9	356	28.2	9.87	2330
SIV	0.151	16.0	325	31.2	63.5	353
SV	0.155	16.1	306	32.8	96.1	224
SVI	0.144	15.8	364	26.9	-7.38	-3080
Ska	0.155	16.0	263	32.9	74.6	249
Skb	0.155	16.0	263	23.9	47.5	284
SG-0	0.168	16.7	253	35.6	41.6	430
SGI	0.154	15.8	261	28.3	64.1	250
SGII	0.158	15.6	215	26.8	37.6	322
SkM	0.160	15.8	217	30.7	49.3	281
SkM*	0.160	15.8	217	30.0	45.8	296
E	0.159	16.1	334	27.6	-31.3	-617
E_σ	0.163	16.0	249	26.4	-36.9	-364
Z	0.159	16.0	330	26.8	-49.8	-373
Z_σ	0.163	15.9	233	26.7	-29.4	-432
Z_σ^*	0.163	16.0	235	28.8	-4.58	-3030
R_σ	0.158	15.6	238	30.6	85.7	179
G_σ	0.158	15.6	237	31.4	94.0	167
MskA	0.154	16.0	314	30.4	57.2	361
SkT6	0.161	16.0	236	30.0	30.8	475
SkP	0.163	16.0	201	30.0	19.5	632
SkSC4	0.161	15.9	235	28.8	-2.17	-6460
SkX	0.155	16.1	271	31.1	33.2	545
Msk7	0.158	15.8	231	27.9	9.36	1460
Bsk1	0.157	15.8	231	27.8	7.15	1908
SLy4	0.160	16.0	230	32.0	45.9	335
SLy7	0.158	15.9	230	32.0	47.2	328
TM1	0.145	16.3	281	37.9	114	215

Table A.1
 Optimal values of the parameters n_0 , w_0 , S_0 , L and F_0 for fixed y and K_0

$-y$	K_0	n_0	$-w_0$	S_0	L	F_0
200	180	0.16931	16.257	32.899	58.296	71.300
200	190	0.16695	16.239	33.154	62.887	70.892
200	200	0.16491	16.227	33.430	67.572	70.534
200	210	0.16298	16.214	33.723	72.421	70.221
200	220	0.16125	16.204	34.037	77.398	69.914
200	230	0.15965	16.193	34.365	82.511	69.539
200	240	0.15793	16.120	34.543	87.488	67.031
200	250	0.15685	16.186	35.113	93.278	69.320
200	260	0.15228	15.932	34.905	99.328	63.190
200	270	0.15200	15.870	34.933	103.42	60.072
200	280	0.15298	16.157	36.349	110.88	68.403
200	290	0.15184	16.153	36.856	117.32	68.297
200	300	0.14880	15.858	36.503	122.66	59.622
200	310	0.14972	16.144	37.939	130.93	68.070
200	320	0.14867	16.139	38.540	138.26	68.006
200	330	0.14772	16.135	39.190	145.92	67.944
200	340	0.14673	16.131	39.904	154.10	67.911
200	350	0.14582	16.130	40.684	162.75	67.969
200	360	0.14444	16.056	41.232	171.28	65.851
220	180	0.16925	16.250	32.350	52.129	71.133
220	190	0.16698	16.234	32.564	56.141	70.709
220	200	0.16489	16.218	32.791	60.264	70.320
220	210	0.16303	16.207	33.031	64.467	69.959
220	220	0.16131	16.196	33.286	68.784	69.625
220	230	0.15969	16.184	33.550	73.214	69.276
220	240	0.15821	16.175	33.835	77.767	68.969
220	250	0.15748	16.184	34.183	82.224	68.520
220	260	0.15412	16.053	34.231	87.496	65.686
220	270	0.15438	16.179	34.850	92.349	69.206

Table A.1—continued

$-y$	K_0	n_0	$-w_0$	S_0	L	F_0
220	280	0.15265	16.003	34.543	96.002	63.371
220	290	0.15128	16.019	35.173	102.16	63.971
220	300	0.15110	16.133	35.917	108.05	67.413
220	310	0.15019	16.135	36.354	113.69	67.388
220	320	0.14856	16.000	36.340	118.60	63.115
220	330	0.14832	16.126	37.295	125.72	67.102
220	340	0.14742	16.123	37.813	132.14	67.039
220	350	0.14651	16.128	38.395	138.97	67.357
220	360	0.14570	16.114	38.963	145.86	66.841
250	180	0.16876	16.191	31.643	45.001	69.337
250	190	0.16694	16.225	31.893	48.399	70.488
250	200	0.16490	16.210	32.071	51.862	70.075
250	210	0.16305	16.197	32.251	55.383	69.669
250	220	0.16136	16.184	32.449	58.988	69.240
250	230	0.15978	16.174	32.655	62.675	68.890
250	240	0.15829	16.154	32.851	66.410	68.193
250	250	0.15707	16.155	33.098	70.239	68.083
250	260	0.15590	16.159	33.388	74.246	68.228
250	270	0.15479	16.129	33.574	78.083	66.874
250	280	0.15364	16.142	33.882	82.331	67.477
250	290	0.15087	15.950	33.612	86.147	62.109
250	300	0.15173	16.132	34.449	90.818	66.855
250	310	0.14900	16.081	34.601	95.985	67.159
250	320	0.14894	16.028	34.781	99.635	63.947
250	330	0.14889	16.113	35.403	104.62	66.202
250	340	0.14818	16.074	35.654	109.08	64.564
250	350	0.14727	16.105	36.144	114.54	65.893
250	360	0.14653	16.103	36.548	119.72	65.769

Table A.1—continued

$-y$	K_0	n_0	$-w_0$	S_0	L	F_0
300	180	0.16915	16.232	31.027	36.685	70.687
300	190	0.16679	16.206	31.127	39.398	69.997
300	200	0.16492	16.201	31.261	42.123	69.789
300	210	0.16304	16.185	31.387	44.919	69.318
300	220	0.16138	16.172	31.522	47.747	68.875
300	230	0.15991	16.164	31.669	50.612	68.492
300	240	0.15845	16.152	31.816	53.547	68.116
300	250	0.15716	16.144	31.977	56.518	67.747
300	260	0.15594	16.135	32.136	59.533	67.382
300	270	0.15487	16.129	32.312	62.595	67.030
300	280	0.15386	16.128	32.498	65.712	66.862
300	290	0.15301	16.134	32.722	68.907	66.850
300	300	0.15309	16.206	33.118	72.109	68.333
300	310	0.15101	16.103	33.093	75.485	65.682
300	320	0.14987	16.058	33.149	78.644	64.466
300	330	0.14883	16.071	33.480	82.484	65.001
300	340	0.14699	15.926	33.240	85.428	60.873
300	350	0.14680	15.964	33.630	89.092	61.549
300	360	0.14746	16.025	34.068	92.411	62.205
350	180	0.16905	16.224	30.543	30.974	70.513
350	190	0.16677	16.201	30.617	33.221	69.869
350	200	0.16472	16.180	30.696	35.495	69.261
350	210	0.16297	16.174	30.811	37.813	69.037
350	220	0.16086	16.131	30.837	40.166	67.933
350	230	0.15979	16.145	31.002	42.498	67.975
350	240	0.15877	16.167	31.189	44.902	68.422
350	250	0.15729	16.138	31.258	47.315	67.474
350	260	0.15608	16.128	31.374	49.775	67.057
350	270	0.15500	16.121	31.503	52.263	66.690

Table A.1—continued

$-y$	K_0	n_0	$-w_0$	S_0	L	F_0
350	280	0.15412	16.143	31.701	54.852	67.309
350	290	0.15305	16.108	31.777	57.343	65.982
350	300	0.15211	16.101	31.917	59.953	65.635
350	310	0.15133	16.099	32.071	62.569	65.373
350	320	0.15117	16.227	32.539	65.599	69.348
350	330	0.14978	16.088	32.384	67.950	64.685
350	340	0.14959	16.073	32.489	70.326	63.401
350	350	0.14785	16.073	32.714	73.757	64.408
350	360	0.14741	16.025	32.734	76.137	62.538
400	180	0.16902	16.219	30.206	26.807	70.423
400	190	0.16675	16.200	30.263	28.736	69.895
400	200	0.16446	16.164	30.287	30.693	69.005
400	210	0.16303	16.173	30.412	32.645	68.967
400	220	0.16138	16.158	30.481	34.628	68.483
400	230	0.15988	16.148	30.566	36.642	68.057
400	240	0.15855	16.138	30.654	38.668	67.603
400	250	0.15728	16.130	30.746	40.727	67.250
400	260	0.15615	16.122	30.845	42.801	66.850
400	270	0.15505	16.113	30.942	44.900	66.429
400	280	0.15406	16.107	31.043	47.016	66.044
400	290	0.15315	16.100	31.156	49.162	65.654
400	300	0.15227	16.095	31.265	51.332	65.344
400	310	0.15146	16.090	31.381	53.526	65.004
400	320	0.15070	16.087	31.508	55.754	64.721
400	330	0.14996	16.081	31.627	58.000	64.364
400	340	0.14938	16.164	31.976	60.648	67.165
400	350	0.14854	16.071	31.895	62.628	63.808
400	360	0.14701	16.095	32.082	65.471	65.588

Table A.1—continued

$-y$	K_0	n_0	$-w_0$	S_0	L	F_0
500	180	0.16895	16.213	29.750	21.131	70.289
500	190	0.16674	16.194	29.786	22.628	69.745
500	200	0.16506	16.201	29.868	24.127	69.843
500	210	0.16324	16.179	29.901	25.644	69.044
500	220	0.16136	16.149	29.914	27.191	68.228
500	230	0.15991	16.141	29.972	28.739	67.851
500	240	0.15856	16.130	30.028	30.302	67.377
500	250	0.15731	16.120	30.085	31.875	66.940
500	260	0.15620	16.112	30.152	33.459	66.504
500	270	0.15513	16.104	30.216	35.060	66.079
500	280	0.15421	16.098	30.288	36.663	65.685
500	290	0.15330	16.092	30.359	38.286	65.293
500	300	0.15243	16.086	30.437	39.934	64.956
500	310	0.15165	16.080	30.511	41.581	64.550
500	320	0.15091	16.076	30.594	43.249	64.240
500	330	0.15022	16.073	30.678	44.930	63.950
500	340	0.14957	16.069	30.765	46.624	63.597
500	350	0.14892	16.063	30.852	48.341	63.250
500	360	0.14912	16.222	31.314	50.399	68.034
600	180	0.16890	16.208	29.461	17.443	70.159
600	190	0.16669	16.188	29.475	18.664	69.602
600	200	0.16470	16.172	29.496	19.899	69.132
600	210	0.16393	16.245	29.692	21.132	70.991
600	220	0.16137	16.148	29.560	22.389	68.204
600	230	0.15990	16.135	29.596	23.651	67.684
600	240	0.15856	16.123	29.634	24.920	67.189
600	250	0.15735	16.114	29.675	26.194	66.714
600	260	0.15626	16.108	29.724	27.476	66.344
600	270	0.15519	16.097	29.766	28.770	65.856

Table A.1—continued

$-y$	K_0	n_0	$-w_0$	S_0	L	F_0
600	280	0.15422	16.091	29.818	30.077	65.479
600	290	0.15336	16.085	29.871	31.381	65.049
600	300	0.15254	16.081	29.930	32.701	64.714
600	310	0.15176	16.075	29.988	34.031	64.339
600	320	0.15106	16.070	30.047	35.362	63.953
600	330	0.15042	16.072	30.118	36.708	63.752
600	340	0.14968	16.061	30.168	38.071	63.287
600	350	0.15232	16.340	30.965	39.528	69.329
600	360	0.14849	16.053	30.297	40.808	62.629
800	180	0.16884	16.203	29.105	12.929	70.077
800	190	0.16688	16.200	29.137	13.823	69.926
800	200	0.16491	16.183	29.142	14.726	69.348
800	210	0.16455	16.283	29.351	15.607	71.847
800	220	0.16132	16.135	29.140	16.558	67.801
800	230	0.15982	16.127	29.147	17.478	67.534
800	240	0.15858	16.118	29.174	18.397	67.030
800	250	0.15734	16.107	29.193	19.327	66.550
800	260	0.15624	16.099	29.217	20.258	66.079
800	270	0.15527	16.092	29.249	21.193	65.645
800	280	0.15432	16.085	29.276	22.133	65.237
800	290	0.15341	16.076	29.305	23.083	64.764
800	300	0.15265	16.073	29.342	24.028	64.400
800	310	0.15186	16.067	29.373	24.983	64.001
800	320	0.15117	16.063	29.414	25.943	63.644
800	330	0.15047	16.057	29.448	26.909	63.268
800	340	0.14983	16.053	29.489	27.881	62.933
800	350	0.14925	16.049	29.529	28.852	62.575
800	360	0.14866	16.041	29.572	29.839	62.127

Table A.1—continued

$-y$	K_0	n_0	$-w_0$	S_0	L	F_0
1000	180	0.16891	16.213	28.929	10.276	70.446
1000	190	0.16656	16.179	28.890	10.985	69.460
1000	200	0.16460	16.164	28.888	11.700	68.969
1000	210	0.16411	16.266	29.106	12.415	71.720
1000	220	0.16127	16.133	28.888	13.136	67.828
1000	230	0.15989	16.124	28.890	13.853	67.378
1000	240	0.15857	16.114	28.907	14.584	66.911
1000	250	0.15738	16.103	28.920	15.314	66.392
1000	260	0.15626	16.095	28.933	16.047	65.958
1000	270	0.15525	16.086	28.950	16.783	65.496
1000	280	0.15433	16.080	28.969	17.520	65.071
1000	290	0.15345	16.074	28.988	18.261	64.677
1000	300	0.15268	16.069	29.012	19.001	64.238
1000	310	0.15191	16.063	29.037	19.752	63.864
1000	320	0.15121	16.059	29.060	20.499	63.503
1000	330	0.15053	16.052	29.085	21.253	63.069
1000	340	0.14991	16.048	29.110	22.008	62.729
1000	350	0.14935	16.045	29.141	22.763	62.395
1000	360	0.14880	16.042	29.171	23.525	62.056
1400	180	0.16872	16.195	28.677	7.2841	69.908
1400	190	0.16657	16.178	28.657	7.7828	69.419
1400	200	0.16460	16.160	28.641	8.2861	68.842
1400	210	0.16291	16.146	28.633	8.7877	68.295
1400	220	0.16130	16.132	28.624	9.2955	67.785
1400	230	0.15979	16.115	28.608	9.8043	67.148
1400	240	0.15867	16.117	28.633	10.311	66.953
1400	250	0.15735	16.097	28.615	10.825	66.220
1400	260	0.15632	16.093	28.625	11.336	65.868
1400	270	0.15527	16.084	28.627	11.852	65.403

Table A.1—continued

$-y$	K_0	n_0	$-w_0$	S_0	L	F_0
1400	280	0.15433	16.075	28.634	12.369	64.909
1400	290	0.15352	16.071	28.645	12.883	64.546
1400	300	0.15269	16.063	28.655	13.405	64.064
1400	310	0.15196	16.058	28.667	13.924	63.663
1400	320	0.15126	16.053	28.681	14.447	63.317
1400	330	0.15065	16.048	28.693	14.965	62.884
1400	340	0.15003	16.044	28.708	15.490	62.512
1400	350	0.14941	16.039	28.713	16.015	62.182
1400	360	0.14889	16.035	28.738	16.544	61.778
1800	180	0.16868	16.193	28.552	5.6423	69.913
1800	190	0.16652	16.174	28.525	6.0275	69.339
1800	200	0.16460	16.158	28.508	6.4145	68.779
1800	210	0.16281	16.142	28.488	6.8046	68.254
1800	220	0.16126	16.129	28.475	7.1940	67.714
1800	230	0.15983	16.116	28.465	7.5857	67.193
1800	240	0.15846	16.104	28.446	7.9788	66.736
1800	250	0.15738	16.098	28.459	8.3715	66.256
1800	260	0.15629	16.090	28.457	8.7665	65.790
1800	270	0.15530	16.082	28.457	9.1619	65.332
1800	280	0.15437	16.074	28.459	9.5591	64.869
1800	290	0.15349	16.065	28.457	9.9567	64.391
1800	300	0.15271	16.058	28.462	10.354	63.912
1800	310	0.15199	16.056	28.471	10.754	63.584
1800	320	0.15129	16.050	28.478	11.155	63.167
1800	330	0.15068	16.046	28.485	11.553	62.780
1800	340	0.15009	16.043	28.498	11.955	62.431
1800	350	0.14948	16.037	28.507	12.361	62.062
1800	360	0.14895	16.032	28.515	12.763	61.648